Journal of
Materials Chemistry B

Multimodal spectroscopic investigation of the conformation and local environment of biomolecules at an electrified interface

Journal:	*Journal of Materials Chemistry B*
Manuscript ID	TB-ART-05-2020-001158.R1
Article Type:	Paper
Date Submitted by the Author:	08-Jul-2020
Complete List of Authors:	Moonitz, Sasha; University of Utah, Chemistry Shepard, Noah; University of Utah, Chemistry Noriega, Rodrigo; University of Utah, Chemistry

Multimodal spectroscopic investigation of the conformation and local environment of biomolecules at an electrified interface

Sasha A Moonitz[1], Noah Shepard[1], Rodrigo Noriega[1,*]

[1] University of Utah, Department of Chemistry, 315 S. 1400 E. Salt Lake City, UT 84112

* Email: noriega@chem.utah.edu

Abstract

The complex and dynamic interfacial regions between biological samples and electronic components pose many challenges for characterization, including their evolution over multiple temporal and spatial scales. Spectroscopic probes of buried interfaces employing mid-infrared plasmon resonances and time-resolved fluorescence detection in the visible range are used to study the properties of polypeptides adsorbed at the surface of a working electrode. Information from these complementary spectroscopic probes reveals the interplay of solvation, electric fields, and ion concentration on their resulting macromolecular conformations.

Introduction

Interfaces are ubiquitous in biological systems and in biomedical devices,[1–4] and such interfacial regions are dynamic environments which evolve over multiple time scales – from sub-picosecond molecular motions to microsecond cellular events and even slower biological and chemical processes.[4–8] Moreover, phase boundaries are often electrically charged and experience strong concentration gradients of ionic solutes.[5] It is within this complex environment that processes involving the assembly of biomolecules at phase boundaries take place – e.g., the formation of bioelectronic interfaces and the growth of biofilms.[3,7,9–11] Because interfaces are critical components in sensors and stimuli delivery devices, it is relevant to develop novel experimental platforms to probe the interactions between conformationally flexible biomolecules, their dynamic solvent environment, and ionic species under the effect of electric fields.

The characterization of interfaces is a challenging feat due in part to their small spatial extent compared to bulk material, the large heterogeneity in their composition and morphology, and their continuous evolution over time. In particular, buried interfaces are difficult to characterize nondestructively and under operating conditions. To date, a variety of tools – from scanning probe microscopy to visible and infrared linear and nonlinear spectroscopies – have been developed to interrogate biological interfaces and measure properties such as their chemical structure,[12,13] morphology,[14–17] and formation kinetics.[17–20] In recent years, it has become clear that advancing our understanding of complex mixtures at heterogeneous interfaces and in the presence of external stimuli requires the combination of multiple experimental techniques that provide complementary information with interfacial sensitivity.[20–23] Importantly, in order to study hierarchical

transformations that link molecular-scale events to phenomena at the mesoscopic and macroscopic scales, characterization tools should be able to probe fast processes (10^{-12}-10^{-6} s). Beyond these temporal resolution and surface-sensitivity requirements, in order to enable the broadest possible applicability it is desirable to pursue experimental platforms that do not impose stringent constraints on materials properties (e.g., nonlinear polarizabilities, HOMO/LUMO level alignment) or on sample geometry (e.g., high surface area, specific crystalline facets).

To this effect, we have developed an experimental platform that combines time-resolved fluorescence spectroscopy with mid-infrared surface plasmon resonances launched by ultrafast laser pulses at an active electrochemical interface. This combination of characterization techniques is made possible by wide band gap degenerate metal oxide semiconductor films (indium tin oxide, ITO), which can simultaneously act as a plasmonic medium with strong resonances in the mid-infrared,[24–32] as the working electrode in an electrochemical cell or biosensor,[33,34] and as a transparent window in the UV-vis-NIR range for optical excitation and fluorescence collection.[35] We employ the capabilities of these two complementary interface-sensitive spectroscopic tools to detect the electric-field assisted adsorption of polypeptide layers at a solid/liquid interface, the changes in their hydration state, and the electric field perturbation of their molecular conformations and solvation environment. The signatures of coupled processes involving the intercalation of solvent molecules and ions in the adsorbed layer and the collective changes in conformation of polypeptide chains are detected by correlating surface plasmon reflectivity with time-resolved fluorescence brightness, lifetime, and anisotropy.

We find that the properties of adsorbed polypeptides are not only dependent on bulk solvent properties, but they can be modulated with interfacial electric fields.

Experimental

Materials and Methods

Materials. Details on the deposition of ITO films, preparation of buffered solutions and samples can be found in the Supporting Information.

Optical and electrical properties of ITO films. After ITO deposition, a subset of sacrificial substrates were characterized with a combination of structural, optical, and electrical measurements. ITO film thicknesses between 120-200 nm were measured with a stylus profilometer (Tencor P-10), and their root-mean-square surface roughness was found to be ≤ 2.15 nm using atomic force microscopy (Bruker Dimension Icon, **Fig. S1**). Spectroscopic ellipsometry was employed to extract complex refractive indices for the film stack (**Fig. S2**). A Drude model was used to describe the ITO optical properties, with typical values for plasma frequency and damping coefficient of $\omega_p = 2.2 - 3.1 \times 10^{15}$ Hz and $\Gamma \sim 2.5 \times 10^{14}$ Hz, respectively (free carrier density $n_e = 0.5 - 1.1 \times 10^{21}\ \mathrm{cm}^{-3}$). Conductivity measurements with a 4-point probe (Microtech RF-1) yield sheet resistances of 10-30 Ω/□, in agreement with thickness and doping values obtained with optical characterization. Substrates had a high transmittance (~85%) in the visible spectral range.

Mid-IR plasmonic response of ITO SPR chips. Reflectivity curves were acquired for ITO SPR chips in contact with simple dielectric media (air, water, methanol). All SPR

measurements were taken in the Kretschmann configuration (**Fig. 1**) – experimental and modeling details are provided in the Supporting Information. The plasmonic behavior of ITO substrates can be described with a simple dielectric stack model yielding similar parameters as those obtained from spectroscopic ellipsometry. Importantly, sharp plasmonic resonances are observed using ultrafast pulsed sources in the mid-IR. Sensitivity estimates (**Fig. S3**) agree with model predictions and enable detection of small changes in interfacial properties, as discussed below.

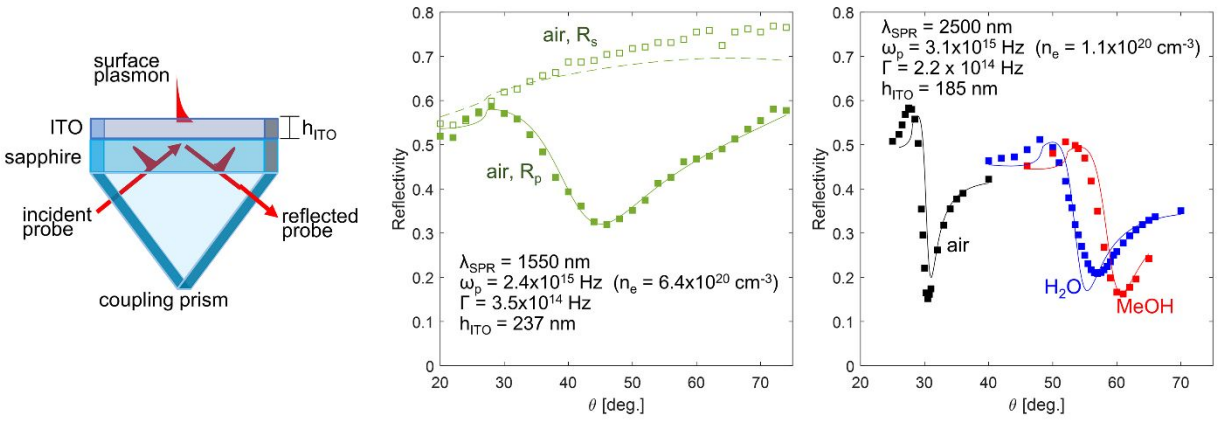

Figure 1. **Surface plasmon resonances in the mid-IR can be supported by degenerately doped ITO films, even when in contact with condensed phases.** The reflectivity of a probe as a function of incident angle is measured in the Kretschmann configuration (left panel). The plasmonic nature of these resonances is evidenced by the characteristic reflectance minimum for incident beams with *p*-polarization but no resonance for *s*-polarized light (center panel). These SPR resonances are much sharper at longer wavelengths, and optimization of experimental geometry and materials parameters enable probing of condensed phases (right panel). Drude metal model parameters for ITO are shown in the center and right panels (ITO films deposited under different conditions). Markers are data, and lines are modeled SPR curves.

SPR measurements of polypeptide adsorption. Before electric-field assisted polypeptide adsorption, a full trace of reflectivity vs. incidence angle is taken in air followed by two curves in solvents of different refractive index (buffer solution and methanol). These

preliminary data serve as a benchmark for the response of each individual ITO mid-IR SPR chip. Using these results, a sensing angle is selected for further data collection (to minimize errors due to detector re-positioning). Changes in reflectivity at constant sensing angle are then measured as a function of voltage and buffer conditions. Surface potentials at the ITO working electrode are applied with a CH Instruments bipotentiostat using a Pt counter electrode and a Ag/AgCl quasi-reference electrode (**Fig. S4**).

Time-resolved fluorescence of adsorbed polypeptide layers. Low-background fluorescence measurements of chromophore-labeled polypeptides adsorbed on ITO were performed using a polarization-resolved ultrafast fluorescence instrument with few modifications from a previously described setup.[36] The electrostatic potential at the ITO surface is controlled with the same electrochemical setup used for SPR measurements. Instrumental and data analysis details are provided in the Supporting Information and **Fig. S5**.

Results and discussion

Field-enhanced adsorption and environment-dependent hydration of adsorbed polypeptides at an electrode. The interfacial adsorption of charged polypeptides under the effect of electric fields has been previously reported using optical waveguide loss spectroscopy and correlated to quartz crystal microbalance experiments.[19,37,38] Here, we exploit the adhesion of poly-L-lysine (PLL) onto an electrified surface to characterize its conformational transformations upon pH changes and as a function of an interfacial electric field. We observe irreversible adsorption of PLL from a high ionic strength

(*I*=1.2 M) pH=11 Britton-Robinson buffer at positive potentials (**Fig. 2**). After adsorption is saturated at large positive surface potentials, no change in reflectivity was observed upon further changes in voltage. These PLL adsorbates cover ~3-10% of the ITO substrate and have a layer height of ~80 nm (**Fig. S6**). Dielectric stack modeling of the SPR response allows the extraction of dielectric constant for the PLL adsorbates (n_{PLL}~1.8-2.7) in agreement with previously reported values for peptide nanostructures.[39] FTIR experiments reveal that dry PLL films exhibit primarily a β-sheet conformation (**Fig. S7**).

Exchange to a pH=7 buffer leads to a much larger increase in the SPR reflectivity. This observation is explained by the well-known pH-mediated change in charge state of lysine residues (from neutral to positively charged upon reducing the pH below ~10.6), concurrent with the hydration of the PLL layer as the polypeptide chains assume a random coil conformation.[40–42,20] Modeling the SPR response using a composite layer including partially hydrated PLL adsorbates (10-20% hydration) shows a ~200 nm interfacial region. In its hydrated state, the polypeptide layer exhibits a small but noticeable electric field-dependent thickness change of ~25 nm, with the larger value at positive surface potentials. The starting and end point for this thickness change depend on the assumed hydration of the PLL adsorbates: 175-200 nm (10% hydration) or 210-235 nm (20% hydration).

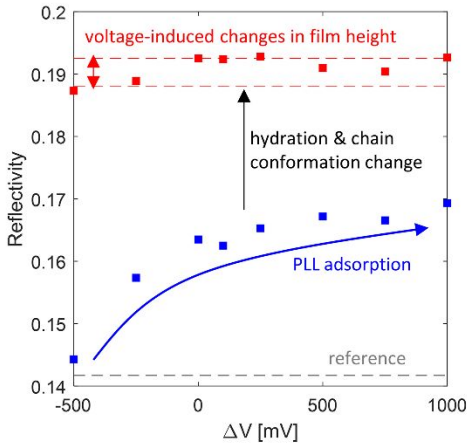

Figure 2. **Surface plasmon reflectivity can detect electric field-assisted adsorption of thin polypeptide layers from aqueous media.** Exchange from a pH=11 to a pH=7 buffer results in hydration-related changes in the charge state and conformation of PLL chains at the interface, with voltage-dependent layer thickness.

These conformational changes are further characterized using time-resolved fluorescence. The local environment at the electrode interface not only affects the conformation of polypeptide chains, it also modulates the concentration of ionic species near the electrode.

Electric field- and solvation-dependent dynamics of fluorescently labeled polypeptide chains. Beyond following time-averaged changes in film conformation, it is informative to probe the dynamic signatures of solvation and chain reorganization by measuring the time-resolved fluorescence dynamics of fluorescein (FITC) chromophores covalently attached to the polypeptide side chains. By collecting time-resolved fluorescence in two orthogonal polarizations simultaneously, it is possible to correlate fluctuations in brightness to changes in dynamic photophysical parameters such as fluorescence lifetime and/or fluorescence anisotropy (**Fig. 3**, details in Supporting Information and **Fig. S8**). We observe substantial brightness fluctuations when the PLL adsorbates are in contact

147 with a pH=7 buffer – up to a 45% increase in detected counts. In high pH buffer much
148 smaller fluctuations are observed (< 20%).

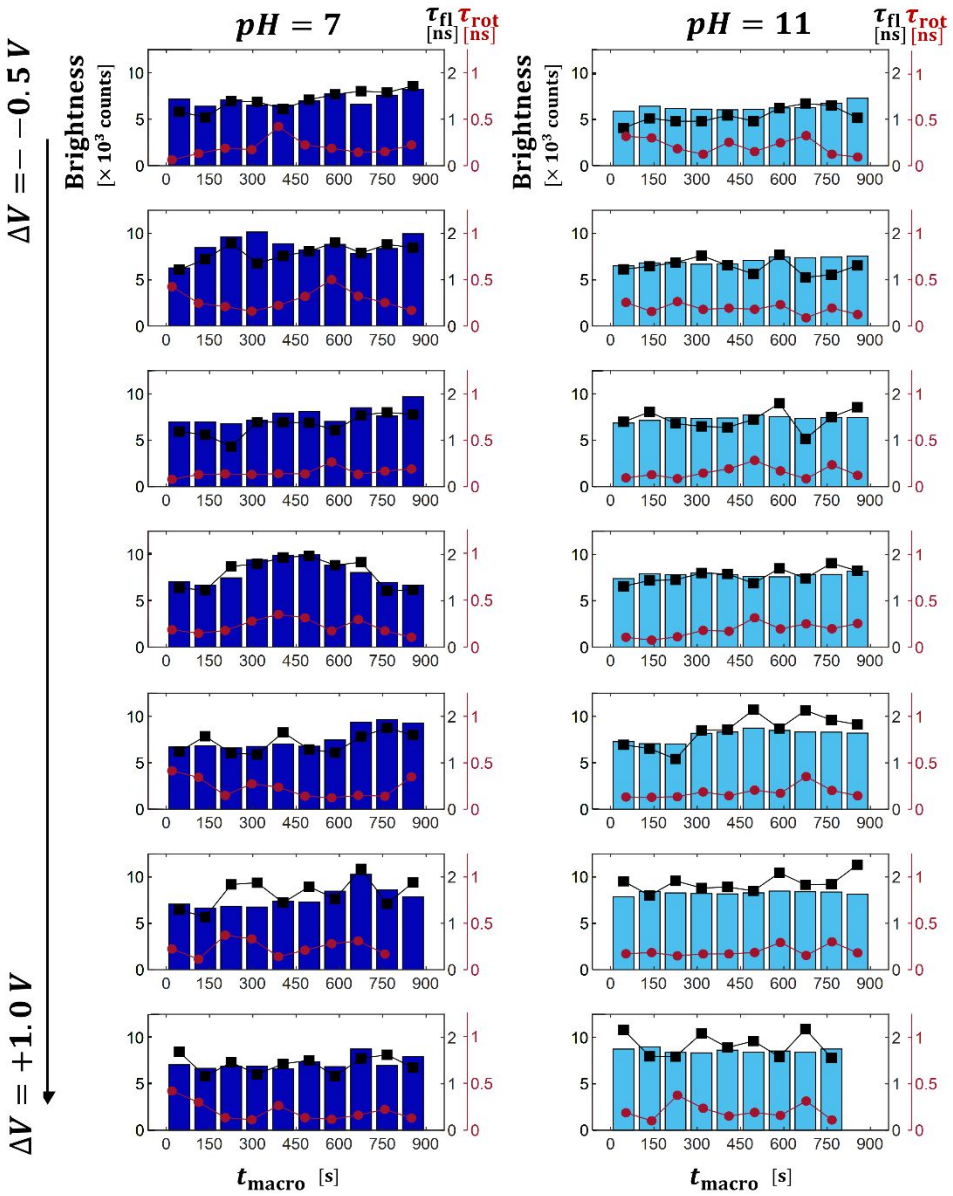

Figure 3. **Trends in time-resolved photoluminescence of adsorbed FITC-PLL on ITO as a function of voltage and pH** show that changes in hydration and chain conformation are related to brightness fluctuations. Brightness trends for FITC-PLL/ITO as a function of interfacial voltage while submerged in a pH=7 buffer (left column), or a pH=11 buffer (right column). In each panel, bars represent brightness, black squares are

the fluorescence lifetime, and red circles are rotational diffusion time. Both buffers have an ionic strength *I*=1.5 M.

It is informative to consider the correlation between brightness and the parameters extracted from time-resolved fluorescence and anisotropy traces (**Fig. S9**). As expected from the trends in **Fig. 3**, brightness fluctuations are strongly correlated with fluorescence lifetime. At pH=11, FITC-labeled PLL displays relatively low fluorescence intensity with a shorter and mostly constant decay lifetime of 1.5 ns. At pH=7, FITC-labeled PLL switches between the dim state observed at pH=11, and a brighter state with a longer fluorescence lifetime of 2 ns. A similar increase in fluorescence lifetime upon solvation of FITC dyes has been also observed in core-shell porous silica nanoparticles.[43] Time-resolved fluorescence anisotropy measurements allow us to monitor the rotational diffusion lifetime. The rotational diffusion dynamics do not depend strongly on pH or voltage, with a rotational diffusion lifetime of ~240 ps. Moderate variations in rotational diffusion lifetime (fastest is ~100 ps, slowest is ~400 ps) are not correlated to the brightness. A positive correlation between brightness and long-time asymptotic value of fluorescence anisotropy – r(∞) – is also observed.

Microenvironment within an adsorbed polypeptide layer at an electrified solid-liquid interface. We interpret the photophysics of FITC-PLL in relation to changes in the local environment of dry or partially hydrated polypeptide adsorbates atop an electrified surface in contact with high ionic strength electrolyte solutions. It is remarkable that these electric field effects are observed for electrolyte solutions with large ionic strengths and correspondingly short electrostatic screening lengths ($\kappa^{-1} < 1\ \mathrm{nm}$). However, it should be noted that solution properties can be markedly different in the bulk vs. at the interface

where the partially hydrated polypeptides exist.[44,45] Additionally, effective electrostatic screening at very high ionic strengths can affect the diffusive properties of charged polypeptides and could be an important contributor to the dynamics observed in this work.[46]

In aggregate, our photophysical observations are reflective of three coupled processes: 1) changes in the solvation state of FITC labels as a result of the overall hydration of the PLL chains, 2) changes in the concentration gradient of ions, and 3) the extension of charged PLL chains. These processes rely on collective motions of polypeptide chains that depend on solution pH and are modulated by the interfacial electric field.

At pH=11, FITC labels are primarily enclosed within dehydrated PLL adsorbates and are thus in a dim state, display a short fluorescence lifetime, and do not exhibit large dynamic changes associated with molecular motion. However, an increase in brightness is observed as the interfacial potential is increased (**Fig. S10**), likely because the interfacial electric field modifies the concentration of H^+ ions within the extended boundary layer at the surface of the dehydrated adsorbates.[44,45] The dependence of FITC emission on H^+ concentration makes it a common pH sensor, and the field-dependent brightness and lifetime at pH=11 (**Fig. S11**) are consistent with FITC bulk properties. However, when considering buffer pH, the overall trends measured here are opposite to what would be expected in bulk solution. The lower fluorescence brightness and shorter fluorescence lifetime in pH=11 (vs. pH=7) suggest that solvation state of the PLL film is the leading determinant of FITC photophysics at the interface.

At pH=7, FITC chromophores are embedded in partially hydrated adsorbates, as observed with SPR experiments. In their solvated state, PLL chains are able to

experience local and collective morphological transformations, which result in large fluctuations in the microenvironment experienced by FITC labels attached to them. These fluctuations in fluorescence brightness and lifetime are primarily due to variations in local solvation. The interfacial electric field does not have a large effect on the average brightness (**Fig. S10**), but a moderate reduction in the brightness fluctuations and a small change in the overall thickness of the film are present at the extremes of the applied surface potential range. These small electric field effects are due to the higher H^+ concentration and the relatively small Debye length compared to a larger portion of the adsorbed layer that is hydrated and contains mobile ions.

The local environment near an electrode surface experienced by adsorbed polypeptide chains and chromophores covalently linked to them is considerably dynamic (i.e., large fluctuations) if they exist in a partially hydrated state in a high ionic strength electrolyte. However, the properties of such a dynamic environment have little dependence on the interfacial electric field because extended polypeptide chains are much longer than the Debye screening length. When the polypeptide chains are not hydrated, they experience a substantially less dynamic environment (i.e., low amplitude fluctuations) but are more sensitive to changes in the interfacial properties as a result of an applied electric field. If the solution atop the FITC-PLL layer is replaced with a lower ionic strength aqueous electrolyte (50 mM vs. 1.5 M, **Fig. S11-12**) the amplitude of the fluctuations is low irrespective of the peptide's hydration state, but a similar behavior for electric-field dependence of interfacial properties is observed.

Conclusions

Electrified interfaces are a complex environment where electrode surfaces, solvent molecules, ions, and free and surface-bound species interact on multiple time scales. The microenvironment at this interface is a critical component in biomedical sensing and therapeutic devices, but also relevant for analytical separations as well as energy conversion and storage. With a combination of plasmonic and fluorescence spectroscopy probes, we gain detailed information on the molecular-scale changes in local environment and conformation at an electrified interface. The broad applicability of these tools is enabled by an instrumental platform with wide material compatibility and optimized spectral, electrical, and morphological properties.

We observe correlated changes in the reflectivity of mid-IR surface plasmon resonances and time-resolved brightness, fluorescence lifetime, and fluorescence anisotropy dynamics that probe poly-L-lysine chains at the interface of an ITO electrode. These observations reveal the interplay between solvent-dependent hydration state and collective rearrangement of adsorbed polypeptides, as well as the electric field-mediated ion concentration at the interface. A noticeable dependence of interfacial properties on applied electric field is observed at a high pH value for which dehydrated polypeptide adsorbates cover the electrode, and these properties are largely static over time. On the contrary, substantial fluctuations in the local solvation environment are observed for partially hydrated peptides at high ionic strength, but with minimal perturbations due to electric fields. A variable layer thickness is also observed upon hydration. Given that implantable bioelectronic devices are often surrounded by large ionic concentrations and at close to neutral pH (e.g., in neural tissue or blood), the presence of large fluctuations

in their interfacial properties can have sizable effects on device performance and stability. The ability to follow coupled changes in interfacial properties enables studies where the contribution of multiple processes (e.g., solvation, chain motion, quenching) can be understood, exploring their co-dependence on external stimuli such as electric fields.

References

(1) Liu, X.; Yuan, L.; Li, D.; Tang, Z.; Wang, Y.; Chen, G.; Chen, H.; Brash, J. L. Blood Compatible Materials: State of the Art. *J. Mater. Chem. B* **2014**, *2* (35), 5718–5738. https://doi.org/10.1039/C4TB00881B.

(2) Maehashi, K.; Katsura, T.; Kerman, K.; Takamura, Y.; Matsumoto, K.; Tamiya, E. Label-Free Protein Biosensor Based on Aptamer-Modified Carbon Nanotube Field-Effect Transistors. *Anal. Chem.* **2007**, *79* (2), 782–787. https://doi.org/10.1021/ac060830g.

(3) Gao, D.; Parida, K.; Lee, P. S. Emerging Soft Conductors for Bioelectronic Interfaces. *Advanced Functional Materials n/a* (n/a), 1907184. https://doi.org/10.1002/adfm.201907184.

(4) Song, E.; Fang, H.; Jin, X.; Zhao, J.; Jiang, C.; Yu, K. J.; Zhong, Y.; Xu, D.; Li, J.; Fang, G.; Du, H.; Zhang, J.; Park, J. M.; Huang, Y.; Alam, M. A.; Mei, Y.; Rogers, J. A. Thin, Transferred Layers of Silicon Dioxide and Silicon Nitride as Water and Ion Barriers for Implantable Flexible Electronic Systems. *Advanced Electronic Materials* **2017**, *3* (8), 1700077. https://doi.org/10.1002/aelm.201700077.

(5) Eftekhari-Bafrooei, A.; Borguet, E. Effect of Electric Fields on the Ultrafast Vibrational Relaxation of Water at a Charged Solid–Liquid Interface as Probed by Vibrational Sum Frequency Generation. *J. Phys. Chem. Lett.* **2011**, *2* (12), 1353–1358. https://doi.org/10.1021/jz200194e.

(6) Lagutchev, A. S.; Patterson, J. E.; Huang, W.; Dlott, D. D. Ultrafast Dynamics of Self-Assembled Monolayers under Shock Compression: Effects of Molecular and Substrate Structure. *J. Phys. Chem. B* **2005**, *109* (11), 5033–5044. https://doi.org/10.1021/jp0450742.

(7) Lee, W.; Kim, D.; Matsuhisa, N.; Nagase, M.; Sekino, M.; Malliaras, G. G.; Yokota, T.; Someya, T. Transparent, Conformable, Active Multielectrode Array Using Organic Electrochemical Transistors. *PNAS* **2017**, *114* (40), 10554–10559. https://doi.org/10.1073/pnas.1703886114.

(8) Hwang, S.-W.; Tao, H.; Kim, D.-H.; Cheng, H.; Song, J.-K.; Rill, E.; Brenckle, M. A.; Panilaitis, B.; Won, S. M.; Kim, Y.-S.; Song, Y. M.; Yu, K. J.; Ameen, A.; Li, R.; Su, Y.; Yang, M.; Kaplan, D. L.; Zakin, M. R.; Slepian, M. J.; Huang, Y.; Omenetto, F. G.; Rogers, J. A. A Physically Transient Form of Silicon Electronics. *Science* **2012**, *337* (6102), 1640–1644. https://doi.org/10.1126/science.1226325.

(9) Bellassai, N.; Marti, A.; Spoto, G.; Huskens, J. Low-Fouling, Mixed-Charge Poly-L-Lysine Polymers with Anionic Oligopeptide Side-Chains. *J. Mater. Chem. B* **2018**, *6* (46), 7662–7673. https://doi.org/10.1039/C8TB01619D.

(10) Chen, X.; Wang, J.; Sniadecki, J. J.; Even, M. A.; Chen, Z. Probing α-Helical and β-Sheet Structures of Peptides at Solid/Liquid Interfaces with SFG. *Langmuir* **2005**, *21* (7), 2662–2664. https://doi.org/10.1021/la050048w.

(11) Rabe, M.; Verdes, D.; Seeger, S. Understanding Protein Adsorption Phenomena at Solid Surfaces. *Advances in Colloid and Interface Science* **2011**, *162* (1), 87–106. https://doi.org/10.1016/j.cis.2010.12.007.

(12) Kishore Sahoo, J.; S. Sirimuthu, N. M.; Canning, A.; Zelzer, M.; Graham, D.; V. Ulijn, R. Analysis of Enzyme-Responsive Peptide Surfaces by Raman Spectroscopy. *Chemical Communications* **2016**, *52* (25), 4698–4701. https://doi.org/10.1039/C5CC09189F.

(13) Kharlampieva, E.; Min Jung, C.; Kozlovskaya, V.; V. Tsukruk, V. Secondary Structure of Silaffin at Interfaces and Titania Formation. *Journal of Materials Chemistry* **2010**, *20* (25), 5242–5250. https://doi.org/10.1039/C0JM00600A.

(14) Dai, B.; Kang, S.; Huynh, T.; Lei, H.; Castelli, M.; Hu, J.; Zhang, Y.; Zhou, R. Salts Drive Controllable Multilayered Upright Assembly of Amyloid-like Peptides at Mica/Water Interface. *PNAS* **2013**, *110* (21), 8543–8548. https://doi.org/10.1073/pnas.1220711110.

(15) Shen, L.; Ulrich, N. W.; Mello, C. M.; Chen, Z. Determination of Conformation and Orientation of Immobilized Peptides and Proteins at Buried Interfaces. *Chemical Physics Letters* **2015**, *619*, 247–255. https://doi.org/10.1016/j.cplett.2014.10.035.

(16) Miller, C. E.; Majewski, J.; Gog, T.; Kuhl, T. L. Characterization of Biological Thin Films at the Solid-Liquid Interface by X-Ray Reflectivity. *Phys. Rev. Lett.* **2005**, *94* (23), 238104. https://doi.org/10.1103/PhysRevLett.94.238104.

(17) Shen, L.; Adachi, T.; Vanden Bout, D.; Zhu, X.-Y. A Mobile Precursor Determines Amyloid-β Peptide Fibril Formation at Interfaces. *J. Am. Chem. Soc.* **2012**, *134* (34), 14172–14178. https://doi.org/10.1021/ja305398f.

(18) Wei, Y.; Latour, R. A. Determination of the Adsorption Free Energy for Peptide−Surface Interactions by SPR Spectroscopy. *Langmuir* **2008**, *24* (13), 6721–6729. https://doi.org/10.1021/la8005772.

(19) Bearinger, J. P.; Vörös, J.; Hubbell, J. A.; Textor, M. Electrochemical Optical Waveguide Lightmode Spectroscopy (EC-OWLS): A Pilot Study Using Evanescent-Field Optical Sensing under Voltage Control to Monitor Polycationic Polymer Adsorption onto Indium Tin Oxide (ITO)-Coated Waveguide Chips. *Biotechnology and Bioengineering* **2003**, *82* (4), 465–473. https://doi.org/10.1002/bit.10591.

(20) Saftics, A.; Prósz, G. A.; Türk, B.; Peter, B.; Kurunczi, S.; Horvath, R. In Situ Viscoelastic Properties and Chain Conformations of Heavily Hydrated Carboxymethyl Dextran Layers: A Comparative Study Using OWLS and QCM-I Chips Coated with Waveguide Material. *Scientific Reports* **2018**, *8* (1), 1–14. https://doi.org/10.1038/s41598-018-30201-6.

(21) Allgeyer, E. S.; Sterling, S. M.; Gunewardene, M. S.; Hess, S. T.; Neivandt, D. J.; Mason, M. D. Combining Total Internal Reflection Sum Frequency Spectroscopy Spectral Imaging and Confocal Fluorescence Microscopy. *Langmuir* **2015**, *31* (3), 987–994. https://doi.org/10.1021/la5036932.

(22) Zhang, C.; Jasensky, J.; Wu, J.; Chen, Z. Combining Surface Sensitive Vibrational Spectroscopy and Fluorescence Microscopy to Study Biological Interfaces. In *Imaging, Manipulation, and Analysis of Biomolecules, Cells, and Tissues XII*; International Society for Optics and Photonics, 2014; Vol. 8947, p 894712. https://doi.org/10.1117/12.2040828.

(23) O'Callahan, B. T.; Park, K.-D.; Novikova, I. V.; Jian, T.; Chen, C.-L.; Muller, E. A.; El-Khoury, P. Z.; Raschke, M. B.; Lea, A. S. In Liquid Infrared Scattering Scanning Near-Field Optical Microscopy for Chemical and Biological Nanoimaging. *Nano Lett.* **2020**, *20* (6), 4497–4504. https://doi.org/10.1021/acs.nanolett.0c01291.

(24) Wang, Y.; Overvig, A. C.; Shrestha, S.; Zhang, R.; Wang, R.; Yu, N.; Negro, L. D. Tunability of Indium Tin Oxide Materials for Mid-Infrared Plasmonics Applications. *Opt. Mater. Express, OME* **2017**, *7* (8), 2727–2739. https://doi.org/10.1364/OME.7.002727.

(25) Rhodes, C.; Franzen, S.; Maria, J.-P.; Losego, M.; Leonard, D. N.; Laughlin, B.; Duscher, G.; Weibel, S. Surface Plasmon Resonance in Conducting Metal Oxides. *Journal of Applied Physics* **2006**, *100* (5), 054905. https://doi.org/10.1063/1.2222070.

(26) Brewer, S. H.; Franzen, S. Indium Tin Oxide Plasma Frequency Dependence on Sheet Resistance and Surface Adlayers Determined by Reflectance FTIR Spectroscopy. *J. Phys. Chem. B* **2002**, *106* (50), 12986–12992. https://doi.org/10.1021/jp026600x.
(27) Agrawal, A.; Johns, R. W.; Milliron, D. J. Control of Localized Surface Plasmon Resonances in Metal Oxide Nanocrystals. *Annual Review of Materials Research* **2017**, *47* (1), 1–31. https://doi.org/10.1146/annurev-matsci-070616-124259.
(28) Franzen, S. Surface Plasmon Polaritons and Screened Plasma Absorption in Indium Tin Oxide Compared to Silver and Gold. *J. Phys. Chem. C* **2008**, *112* (15), 6027–6032. https://doi.org/10.1021/jp7097813.
(29) Franzen, S.; Rhodes, C.; Cerruti, M.; Gerber, R. W.; Losego, M.; Maria, J.-P.; Aspnes, D. E. Plasmonic Phenomena in Indium Tin Oxide and ITO-Au Hybrid Films. *Opt. Lett., OL* **2009**, *34* (18), 2867–2869. https://doi.org/10.1364/OL.34.002867.
(30) Losego, M. D.; Efremenko, A. Y.; Rhodes, C. L.; Cerruti, M. G.; Franzen, S.; Maria, J.-P. Conductive Oxide Thin Films: Model Systems for Understanding and Controlling Surface Plasmon Resonance. *Journal of Applied Physics* **2009**, *106* (2), 024903. https://doi.org/10.1063/1.3174440.
(31) Rhodes, C.; Cerruti, M.; Efremenko, A.; Losego, M.; Aspnes, D. E.; Maria, J.-P.; Franzen, S. Dependence of Plasmon Polaritons on the Thickness of Indium Tin Oxide Thin Films. *Journal of Applied Physics* **2008**, *103* (9), 093108. https://doi.org/10.1063/1.2908862.
(32) Tandon, B.; Agrawal, A.; Heo, S.; Milliron, D. J. Competition between Depletion Effects and Coupling in the Plasmon Modulation of Doped Metal Oxide Nanocrystals. *Nano Lett.* **2019**, *19* (3), 2012–2019. https://doi.org/10.1021/acs.nanolett.9b00079.
(33) Benck, J. D.; Pinaud, B. A.; Gorlin, Y.; Jaramillo, T. F. Substrate Selection for Fundamental Studies of Electrocatalysts and Photoelectrodes: Inert Potential Windows in Acidic, Neutral, and Basic Electrolyte. *PLOS ONE* **2014**, *9* (10), e107942. https://doi.org/10.1371/journal.pone.0107942.
(34) Aydın, E. B.; Sezgintürk, M. K. Indium Tin Oxide (ITO): A Promising Material in Biosensing Technology. *TrAC Trends in Analytical Chemistry* **2017**, *97*, 309–315. https://doi.org/10.1016/j.trac.2017.09.021.
(35) Transparent electrodes for organic optoelectronic devices: a review https://www.spiedigitallibrary.org/journals/Journal-of-Photonics-for-Energy/volume-4/issue-1/040990/Transparent-electrodes-for-organic-optoelectronic-devices-a-review/10.1117/1.JPE.4.040990.full?SSO=1 (accessed Apr 20, 2020).
(36) Jonely, M.; Noriega, R. Role of Polar Protic Solvents in the Dissociation and Reactivity of Photogenerated Radical Ion Pairs. *J. Phys. Chem. B* **2020**, *124* (15), 3083–3089. https://doi.org/10.1021/acs.jpcb.9b11299.
(37) Van Tassel, P. R. Polyelectrolyte Adsorption and Layer-by-Layer Assembly: Electrochemical Control. *Current Opinion in Colloid & Interface Science* **2012**, *17* (2), 106–113. https://doi.org/10.1016/j.cocis.2011.08.008.
(38) Choi, J.-H.; Kim, S.-O.; Linardy, E.; Dreaden, E. C.; Zhdanov, V. P.; Hammond, P. T.; Cho, N.-J. Influence of PH and Surface Chemistry on Poly(l-Lysine) Adsorption onto Solid Supports Investigated by Quartz Crystal Microbalance with Dissipation Monitoring. *J. Phys. Chem. B* **2015**, *119* (33), 10554–10565. https://doi.org/10.1021/acs.jpcb.5b01553.
(39) Handelman, A.; Apter, B.; Shostak, T.; Rosenman, G. Peptide Optical Waveguides. *Journal of Peptide Science* **2017**, *23* (2), 95–103. https://doi.org/10.1002/psc.2944.
(40) Davidson, B.; Fasman, G. D. The Conformational Transitions of Uncharged Poly-L-Lysine. α Helix-Random Coil-β Structure*. *Biochemistry* **1967**, *6* (6), 1616–1629. https://doi.org/10.1021/bi00858a008.

(41) Cieślik-Boczula, K. Alpha-Helix to Beta-Sheet Transition in Long-Chain Poly-l-Lysine: Formation of Alpha-Helical Fibrils by Poly-l-Lysine. *Biochimie* **2017**, *137*, 106–114. https://doi.org/10.1016/j.biochi.2017.03.006.
(42) Wang, Y.; Chang, Y. C. Synthesis and Conformational Transition of Surface-Tethered Polypeptide: Poly(l-Lysine). *Macromolecules* **2003**, *36* (17), 6511–6518. https://doi.org/10.1021/ma034093r.
(43) Santra, S.; Liesenfeld, B.; Bertolino, C.; Dutta, D.; Cao, Z.; Tan, W.; Moudgil, B. M.; Mericle, R. A. Fluorescence Lifetime Measurements to Determine the Core–Shell Nanostructure of FITC-Doped Silica Nanoparticles: An Optical Approach to Evaluate Nanoparticle Photostability. *Journal of Luminescence* **2006**, *117* (1), 75–82. https://doi.org/10.1016/j.jlumin.2005.04.008.
(44) Klitzing, R.; Moehwald, H. Proton Concentration Profile in Ultrathin Polyelectrolyte Films. *Langmuir* **1995**, *11* (9), 3554–3559. https://doi.org/10.1021/la00009a044.
(45) Chen, A. W.; Briseno, A. L.; Santore, M. M. Tunable Fluorescence Quenching near the Graphene-Aqueous Interface. *Journal of Colloid and Interface Science* **2017**, *506*, 76–82. https://doi.org/10.1016/j.jcis.2017.07.019.
(46) Hong, L.; Granick, S. Charged Polypeptide Diffusion at a Very High Ionic Strength. *Journal of Polymer Science Part B: Polymer Physics* **2005**, *43* (23), 3497–3502. https://doi.org/10.1002/polb.20662.

Conflict of Interest

There are no conflicts of interest to declare.

Acknowledgments

The authors acknowledge use of equipment at the Utah Nanofabrication Facility and the Lassonde Entrepreneur Institute at the University of Utah. N.S. was supported from funds from the University of Utah NSF REU program (NSF REU grant 1659579).

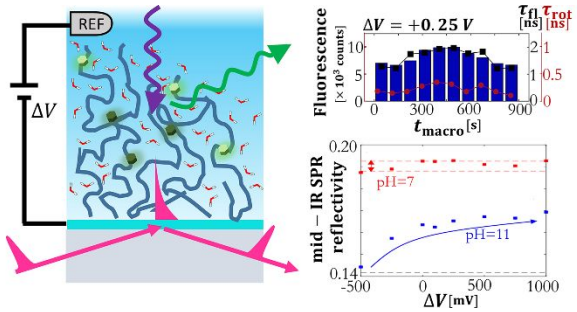

A combination of mid-infrared plasmons and time-resolved fluorescence are used to probe biomolecules at a buried electrochemically active interface.